

SELF-CONSISTENT SIMULATION OF AN INTERNAL ION SOURCE PLASMA MENISCUS AND ITS EXTRACTED SPACE CHARGE DOMINATED BEAM IN THE CYCLOTRON CENTRAL REGION *

G. D'Agostino[†], Istituto Nazionale di Fisica Nucleare-Laboratori Nazionali del Sud, Catania, Italy
 W. Kleeven, Ion Beam Applications (IBA), Louvain-la-Neuve, Belgium
[†]also at Ion Beam Applications (IBA), Louvain-la-Neuve, Belgium

Abstract

Central region design simulations for cyclotrons with internal ion source are often complicated by the fact that the initial particle phase space distribution is not well known. Especially for high-intensity cyclotrons, one would like to have a quantitative self-consistent approach for a more accurate simulation of the beam extracted from the ion source and its acceleration in the first accelerating gaps under space charge conditions. This paper proposes some new ideas and methods for this problem. The simulation approach has been developed at IBA for the high-intensity compact self-extracting cyclotron in the EU-H2020-MSCA InnovaTron project. Detailed results of simulations on plasma meniscus and space charge dominated beam extracted from it and accelerated in the cyclotron centre are shown in the paper.

INTRODUCTION

At IBA a high-intensity compact self-extracting cyclotron, called InnovaTron, is being studied. The machine is a promising tool for large-scale production of medical radioisotopes. Self-extraction allows spontaneous beam extraction. It is based on a very steep fall-off of the magnetic field near the outer pole radius [1]. First harmonic coils increase the turn-separation at extraction. A 14 MeV proton cyclotron build by IBA in 2000 provided the proof-of-principle for this extraction method (extracted beam currents up to 2 mA) [2]. However, rather poor beam quality was observed and the extraction efficiency was limited to about 80% at low intensities. Increase of the dee-voltage ripple resulting from the noisy PIG-source and beam-loading led to an extraction efficiency of about 70%-75% at higher intensities. Main goals set for the project are: i) improvement and optimization of the magnet, extraction elements and central region, ii) space charge simulations, iii) improvement of turn-separation at extraction. Proton currents up to 5 mA are aimed for.

Here, we discuss detailed results obtained for central region studies including space charge in beam dynamics simulations. Space charge plays an important role already during the process of bunch formation in the first gap. It also induces a vortex motion during beam acceleration and an increase of energy spread in the bunch [3]. Simulation results obtained for magnet optimization and a new IBA tool for automated optimization of cyclotron settings are also discussed.

* Work supported by the European Union's Horizon 2020 research and innovation programme under the Marie Skłodowska-Curie grant agreement No 886190.

[†] grazia.dagostino@lns.infn.it

MAGNET OPTIMIZATION

Figure 1 shows the main features of the prototype. The pole gap has a quasi-elliptical shape, allowing for the steep fall-off of the magnetic field (Fig. 1 (a)) by the machining of a groove on the long pole (on which the beam is extracted) at a radius where the gap is small (Fig. 1 (b)). Figure 1 (c) shows one of the harmonic coils. A gradient corrector is used for radial and vertical focusing of the extracted beam. Parts of the beam that are not properly extracted are intercepted by a beam separator shown in Fig. 1 (d). The extraction path in the machine is shown in Fig. 1 (e). More details are in [2].

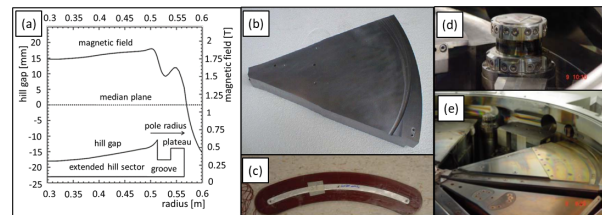


Figure 1: The prototype of the self-extracting cyclotron.

The following improvements have been implemented as compared to the prototype: i) the magnet (and also the accelerating structure) has perfect 2-fold symmetry. This allows irradiation of two targets stations at opposite exit ports and to place two internal ion sources. The latter will increase cyclotron reliability and uptime; ii) the groove in the extraction path is replaced by a "plateau" (Fig. 2 (a)). This reduces the strong sextupole component in the extraction path and improves the extracted beam quality. Figure 2 (b) shows the magnetic field along a line that bisects the long and short poles as shown in Fig. 2 (a); iii) the pole gaps still have a quasi-elliptical shape, decreasing towards larger radii, but the iso-gap contours follow equilibrium orbits. This enables a steeper transition from the internal stable orbit towards the non-stable extracted orbit; iv) an improved gradient corrector has been designed for radial focusing of the extracted beam (Fig. 2 (c,d)).

Figure 2 (e) is a view on the lower half of the magnet developed in Opera3D and shows the harmonic coils (in red), the gradient correctors (in green) and the beam separators (in yellow). The dees (in light blue) are also shown. A beam simulation of the last 5 turns superimposed on the FEM model is shown in Fig. 2 (f). Automatic and parametrized FEM models have been developed for the magnet but also for the central region. More details are given in [4].

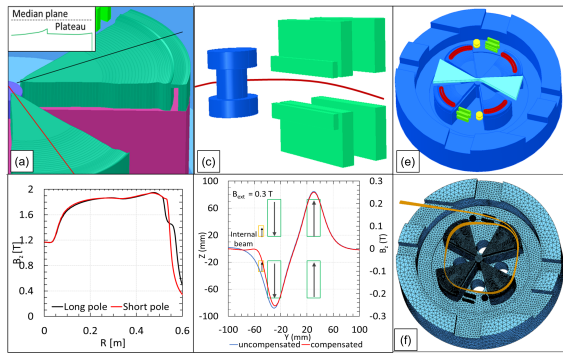


Figure 2: InnoVaTron improved magnet design.

CENTRAL REGION STUDIES

We do an effort for a self-consistent simulation of the space charge dominated beam in the central region. This method consists of three steps. In the first step, the SCALA space charge solver of Opera3D is used to find the plasma meniscus of the ion source. In the second step, the same central region model is solved again, but now with the TOSCA electrostatic solver of Opera3D. Here the meniscus surface is put at ground potential. This provides the 3D electric field map everywhere in the central region, including the source-puller gap. In the third step, the beam extracted from the meniscus is simulated in the 3D field map using the self-consistent in-house space-charge code AOC [5]. This code has been extended to also simulate the bunch formation process in the first gap. More details can be found in [6].

SCALA Simulations

The plasma-free boundary module of SCALA calculates the plasma meniscus and the extracted beam phase space and current density on the meniscus in a DC electric field. SCALA does not solve the plasma itself: the meniscus surface is determined by the Child-Langmuir condition where the external electric field on the surface is cancelled by the space charge electric field. The surface is found in an iterative process. The electric field in a cyclotron central region is not DC but RF. The RF frequency, however, is so high that it will be impossible for the plasma meniscus to follow it, in its motion. The maximum velocity of a material wave is roughly equal to the speed of sound in the material which, for a plasma, will be close to the Bohm-velocity $v_B = \sqrt{kT_e/m_p}$, where T_e is the plasma electron temperature and m_p is the proton mass. Assuming $kT_e \approx 10$ eV we find that the meniscus could move only about 0.1 mm in a quarter of the wave period at 70 MHz. So, it seems that the meniscus will move only weakly in the RF electric field; we therefore make the assumption that the meniscus shape and position can be found by solving the problem for the rms-value of the gap-voltage. It is clear that this is a strong assumption and an important simplification which we can, at this point, not further validate.

For the solution of the SCALA problem we only need to model the local geometry of the source-puller gap. Our

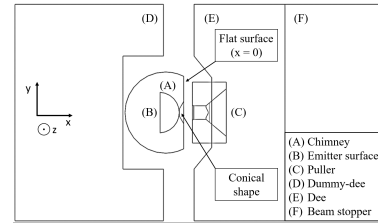


Figure 3: Top view of the SCALA source-puller model.

example is shown in Fig. 3. In this geometry the puller (C) and the dee (E) are placed at high (negative) potential and the chimney (A) and the dummy-dee (D) are at ground potential. The ion source full slit aperture in our example is $\Delta y \times \Delta z = 1 \times 8$ mm². SCALA launches beamlets from the (flat) emitter surface (B), which move to the right towards the ion source slit. At this position, space charge builds up which limits the flow of extracted particles. Besides the geometry, the two important parameters in the simulation are i) the dee-voltage V_{dee} and ii) the emitter current density J_{emit} . Two additional but less critical parameters are iii) the electron temperature T_e and iv) the meniscus voltage V_m . Figure 4 shows examples of four different cases: a) ($V_{dee}=42.1$ kV, $J_{emit}=0.4$ A/cm²), b) $V_{dee}=9.5$ kV, $J_{emit}=0.4$ A/cm²), c) ($V_{dee}=38.9$ kV, $J_{emit}=0.2$ A/cm²) and d) ($V_{dee}=38.9$ kV, $J_{emit}=2$ A/cm²). The first column in the figure is a vertical section through the chimney and shows the position and shape of the meniscus (only the upper half is shown). The middle column shows the vertical beam profile (seen from the $-y$ direction) and the right column shows the horizontal beam profile (seen from the $+z$ direction). The extracted DC currents for the four cases are 100 mA (a), 36.7 mA (b), 67.4 mA (c) and 222 mA (d).

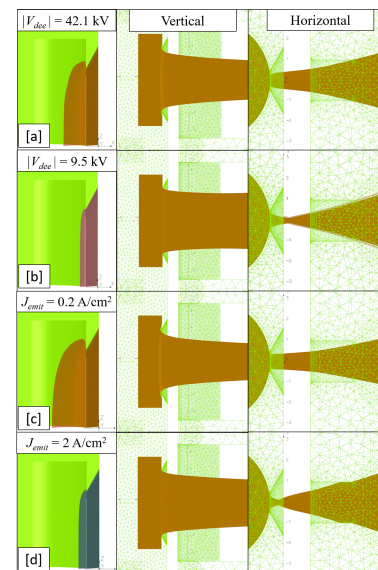


Figure 4: Examples of meniscus shape and beam projections.

A close inspection shows that the extracted current is (almost perfectly) proportional to the surface of the meniscus times the emitter current density. The beamlets cross the

meniscus (almost perfectly) perpendicularly and the flow is (almost perfectly) laminar. It is seen that higher V_{dee} pushes the meniscus to the left and higher J_{emit} pushes the meniscus to the right. Horizontally the beam is strongly converging, with an (over-) focus close to the slit and vertically the beam is weakly converging. This relates directly to the slit dimensions which make that the meniscus is strongly curved in the xy -plane and much more flat in the xz -plane.

Figure 5 shows the extracted current and meniscus position as a function of the four parameters V_{dee} , J_{emit} , T_e and V_m . The position is the distance between the extreme meniscus x -coordinate and the intersection between x -axis and plasma chamber cylinder.

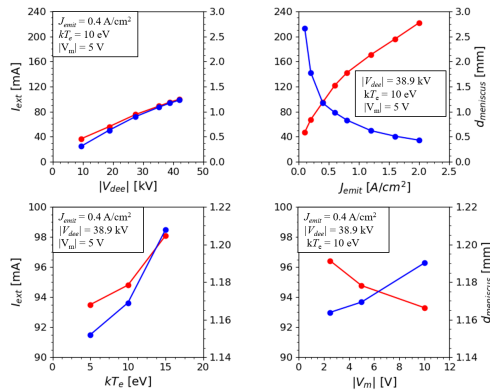


Figure 5: DC extracted current (red) and meniscus position (blue) as function of the four main parameters.

TOSCA Simulations

We extract from the beamlets calculated by SCALA (those who are extracted from the ion source) the particle position coordinates, the velocity components and the beamlet current at the meniscus intersection. These data are used to fit the meniscus x -coordinate, the transverse divergencies (y' , z') and the beamlet currents as a function of y and z . The latter two are considered as independent variables. We use a double polynomial fit up to order 7 (the sum of the y and z exponents) and take into account the symmetry: x is even in y and z ; y' is odd in y and even in z ; z' is even in y and odd in z . This allows to represent the surface of the meniscus as a wire-edge structure with a triangular mesh. This surface is included in the TOSCA model of the central region, where it is put at ground potential (see Fig. 6). With this, one can simulate precisely the value and shape of the 3D electric field in the source-puller gap. The representation also allows to create a file with particle starting conditions for tracking, when y and z are generated randomly and the other variables (x , y' , z') are calculated from the fits.

Figure 7 shows projections of the fitted phase space on the planes xy , xz , yy' , zz' . Three cases are shown: $V_{dee}=38.9$ kV, $J_{emit}=0.4$ A/cm² (green), $V_{dee}=18.8$ kV, $J_{emit}=0.4$ A/cm² (blue), $V_{dee}=38.9$ kV, $J_{emit}=2$ A/cm² (red).

Figure 8 shows in (a) the TOSCA electric field in the source-puller gap for three different cases. One case is for

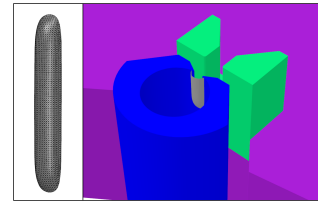


Figure 6: Modeling of the plasma meniscus in TOSCA.

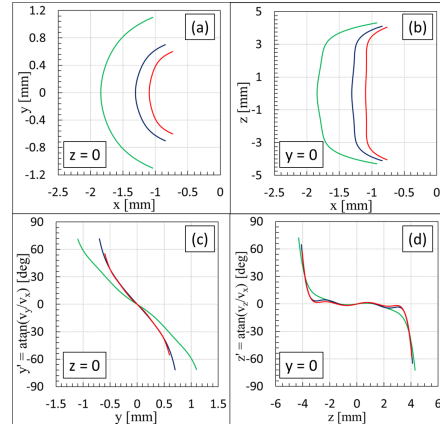


Figure 7: Fitted phase space projections.

the chimney with the conical shape as shown in Fig. 3; for the other two cases, this cone is not present. The meniscus was calculated at $V_{dee}=35.3$ kV for the first case (blue curve) and 18.8 kV for the other two cases. For all three cases, the electric field drops quickly in the space in between the meniscus and the chimney slit ($x < x_{slit}$). As a consequence, the particles must leave early from the meniscus surface in order to be able to cross the gap. This is illustrated in figures (b-d). They show the particle energy gain as a function of time for different starting RF phases ranging from -180° (the moment of zero dee-voltage) up to -130° in steps of 5° (with $V_{dee}=55$ kV). Later starting phases are not properly accelerated by the central region. The worst case is (b) where the energy gain is the lowest and the energy spread is the largest. For this case, the electric field near the meniscus is the lowest and the particles are lost after a few turns in the central region. For cases (c) and (d) the electric field near the meniscus is higher and a phase range of about 40° can be accepted and accelerated. Case (c) is the best as it has good energy gain and the smallest energy spread.

Space Charge in AOC

In the default use of AOC, the full 6D phase space of the initial particles in the bunch must be specified. Recently, a new option has been added in AOC for simulating the formation of the bunch extracted from the ion source meniscus. In this case, the particle properties on the meniscus must be defined and also the number of time-steps that are needed to complete the bunch formation. The bunch will be sliced according to the number of time-steps. For each new step, the bunch is re-defined by adding the additional slice and

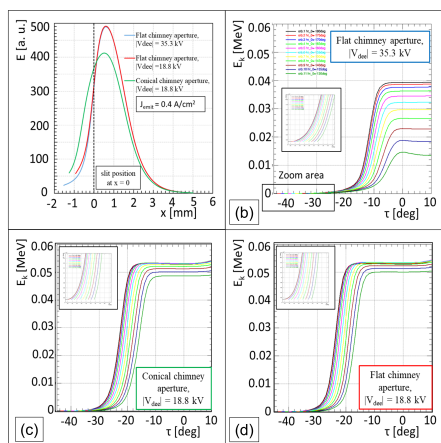


Figure 8: Electric field and energy gain in the first gap.

then advanced using the iterative process. After completing the formation of the bunch, it is continued in the usual way.

FULL BEAM TRACKING

We track a full beam through the central region shown in Fig. 9. The position and orientation of the ion source and the first few accelerating gaps in this central region are optimized in order to obtain good beam centering and good vertical electric focusing. Some additional tools have been made in AOC that allow to slightly rotate/translate the central region geometry without the need to each time solve its 3D FEM model. The collimators (shown in blue) are optimized to limit the accelerated RF phase range to about 40° and by so to remove particles that would otherwise be lost at higher energies. Note that the beam shown in Fig. 9 only includes the "successful" particles. The starting beam, obtained from a SCALA simulation ($J_{emit}=0.4 \text{ A/cm}^2$ and $V_{dee}=18.8 \text{ kV}$) and representing a starting average current of 100 mA on the meniscus, is sampled with 100000 particles in a RF phase range between -180° and 0° .

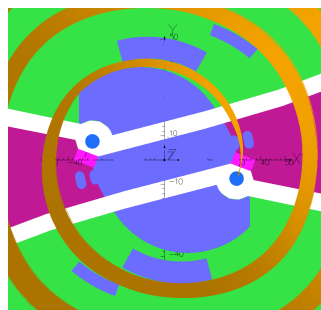


Figure 9: The 2-fold rotational symmetric central region.

Figure 10 shows transmission (a), centering (b), vertical beam size (c) and vertical emittance (d) of the accelerated beam during the first 25 turns. In the representation shown, the particles are binned according to their RF starting phase on the meniscus in four groups of each 10° wide. Only particles in the phase range between -180° and -140° are accepted. The particles must leave early from the meniscus

as explained before. Figure 10 (a) shows that there are high losses in the first 2 turns. This is not only due to the unfavorable transit time but also to the strong over-focusing action in the horizontal plane at the ion source exit (see Fig. 4). Only about 1.7% of the particles is accepted, corresponding to an average beam current of 1.7 mA. The losses are distributed as follows: about 88.7% on the chimney+puller+puller collimators, about 5.8% in the phase selecting collimators and about 3.9% vertically on the dees and dummy-dees. Beyond the second turn all beam properties stabilize.

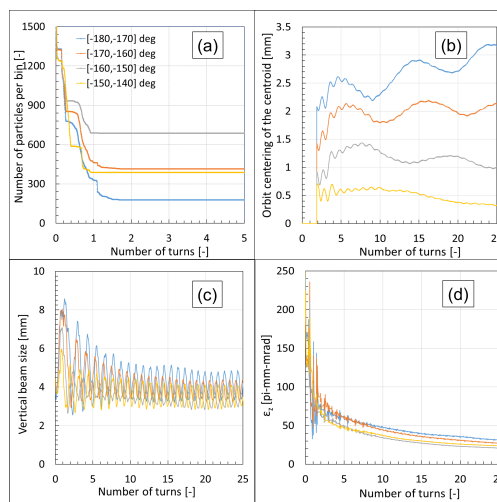


Figure 10: Beam rms properties, binned according to RF starting phase: (a) transmission, (b) beam centroid off-centering, (c) vertical beam size (2σ value), (d) normalized vertical emittance (2σ value).

Figure 11 (a) shows the shape of the accelerated bunches by their projection on the xy-plane, followed during 25 turns at moments when the RF phase equals zero. In another (earlier) simulation, we started a bunch just beyond the source-puller gap with an average beam current of 5 mA, horizontal and vertical emittances of about $20 \pi \text{ mm-mrad}$ (1σ) and a total bunch length of about 3 mm (corresponding to 30° RF phase width). The shape of the bunches for this case is shown (for the first 20 turns) in Figure 11 (b). Here we observe the appearance of circular bunches (with a tail however) which probably is due to the well-known vortex motion [3], turned on by high space charge forces.

Optimization of Cyclotron Settings

Extracted beam optimization is a difficult and tedious process as it depends on multiple parameters (for example harmonic coil settings, dee-voltage, collimator geometry, etc.) and requires full beam tracking (if possible with space charge) from the ion source up to the cyclotron exit. In order to facilitate this process an optimization program (project_optimizer) was written. This program uses standard optimization routines to optimize a task (project). The task is defined by a user-defined script which is executed by the program in an iterative process. It reads new values of independent variables as suggested by the program,

Content from this work may be used under the terms of the CC-BY-4.0 licence (© 2022). Any distribution of this work must maintain attribution to the author(s), title of the work, publisher, and DOI

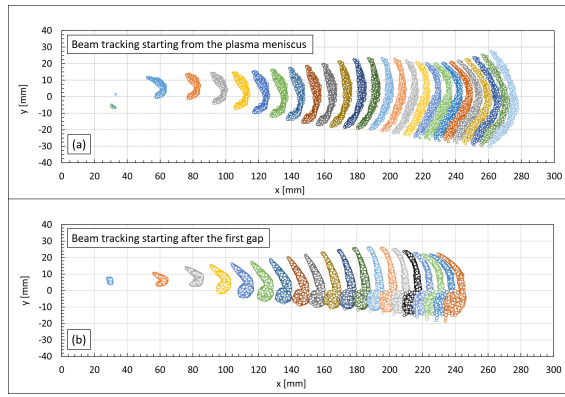


Figure 11: XY projection of accelerated bunches started (a) on the ion source meniscus and (b) after the first gap.

executes the task and writes its results (new values of the objectives) to a file. The program then resumes and compares the results of the script with the (user defined) objectives in order to calculate the fitting error and suggest new values for the variables. This process is repeated until the fitting error is smaller than a given tolerance. In the present study, the script reads all AOC input data and adjusts input field maps as needed. Then, it runs AOC and post-processes its results to extract the objective values. Three standard multiple dimension optimization routines have been implemented (Downhill Simplex Method, Direction SET Powell Method and Simulated Annealing Method).

Extraction efficiency [%]	Harmonic coils currents on the long poles							
	Dee voltage 55.17 KV	-0.35	-0.3	-0.25	-0.2	-0.15	-0.1	
1 st exit part	Harmonic coils current on the short poles	-0.35	59.2	63.1	68.5	76.0	78.7	78.4
		-0.3	59.8	67.0	78.4	82.1	82.2	81.1
		-0.25	60.9	77.2	87.7	87.9	84.9	84.3
		-0.2	81.8	89.6	89.4	89.2	83.7	69.0
		-0.15	91.3	87.3	82.2	68.5	52.3	45.7
		-0.1	76.9	66.3	65.0	72.5	67.6	12.6

Figure 12: Optimization of extraction efficiency.

The process has been tested (without space charge) for a beam of 2000 particles, tracked from the ion source position up to extraction. The starting conditions at the ion source were taken as: $E=100$ eV, $\epsilon_x=125 \pi$ mm-mrad, $\epsilon_z=500 \pi$ mm-mrad, slit aperture $w \times h=1 \times 4$ mm² and starting RF phases $-145^\circ < \Phi < -115^\circ$. The settings of the two pairs of harmonic coils were optimized by `project_optimizer` to obtain maximum extraction efficiency on the first exit port. We found an extraction efficiency of 91% with 7.7% losses on the first beam separator and 1.3% extracted towards the second exit port. Figure 12 illustrates the process of optimization of extraction efficiency as function of harmonic coil settings. Note that this case was still done "by hand".

Figure 13 shows the extracted phase space just beyond the beam separator. At this point we find (1σ) emittances and energy spread of: $\epsilon_x=104 \pi$ mm-mrad, $\epsilon_z=1.25 \pi$ mm-mrad, $\Delta E/E=0.44\%$. As can be seen, there is a large X vs Z asymmetry and the vertical emittance is nicely linear. For the self-extracting cyclotron, good turn separation helps to obtain high extraction efficiency. Turn-separation may be

reduced or lost if the RF dee-voltage is rippled. At high beam intensities this may happen due to beam loading of the RF cavity, if the injected beam intensity is noisy. Internal ion sources indeed are rather noisy. Figure 13 (c,d) shows the extraction efficiency and the beam energy spread as a function of a simulated dee-voltage ripple. It is seen that the RF control system should keep this ripple as low as possible.

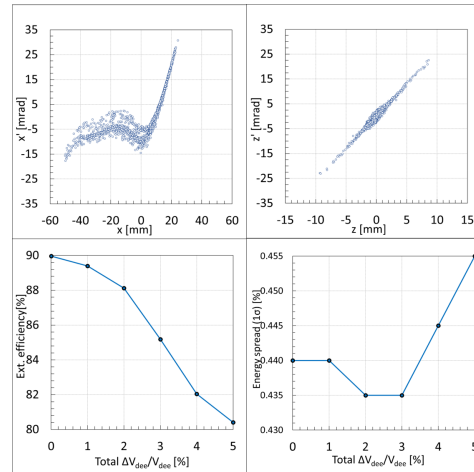


Figure 13: Extracted emittances and dependence of extraction efficiency and energy spread on dee-voltage ripple.

CONCLUSION

We developed new tools i) for the study of space charge beams extracted from the plasma meniscus and bunch formation in the source-puller gap and ii) for automated optimization of cyclotron settings aiming at highest extraction efficiency. Studies are planned to see if the turn-separation at extraction can be further improved.

REFERENCES

- [1] W. Kleeven, "Isochronous cyclotron and method of extraction of charged particles from such cyclotron", Patent No.: US 6,683,426 B1, 27 January 2004.
- [2] W. Kleeven *et al.*, "The IBA self-extracting cyclotron project", in *Proc. Nukleonika*, vol. 48, supplement 2, pp. S59-S67, 2003.
- [3] W. Kleeven, "Some examples of recent progress of beam-dynamics studies for cyclotrons", in *Proc. Cyclotrons'16*, Zurich, Switzerland, Sep. 2016, pp. 244-250. doi:10.18429/JACoW-Cyclotrons2016-WEA01
- [4] G. D'Agostino *et al.*, "InnovaTron: an innovative high-Intensity industrial cyclotron for production of Tc-99m and other frontier medical radioisotopes", in *Proc. IPAC'21*, Campinas, SP, Brazil, May 2021, pp. 1841-1844. doi:10.18429/JACoW-IPAC2021-TUPAB188
- [5] W. Kleeven *et al.*, "AOC, A beam dynamics design code for medical and industrial accelerators at IBA", in *Proc. IPAC'16*, Busan, Korea, May 2016, pp. 1902-1904. doi:10.18429/JACoW-IPAC2016-TUPOY002
- [6] G. D'Agostino and W. Kleeven, "Beam dynamics and space charge studies for the InnovaTron cyclotron", *ICFA Newsletter #84 on Dynamics of High Power and High Energy Cyclotrons*, Ed. Rick Baartman, to be published in *J. Instrum.*